

# Slow Magnetoacoustic Oscillations in the Microwave Emission of Solar Flares

S. Kim

*Nobeyama Solar Radio Observatory / NAOJ, Nagano 384-1305, Japan*

`sjkim@nro.nao.ac.jp`

and

V. M. Nakariakov

*Physics Department, University of Warwick, Coventry, CV4 7AL, UK*

*Central Astronomical Observatory of the Russian Academy of Sciences at Pulkovo, 196140  
St Petersburg, Russia*

and

K. Shibasaki

*Nobeyama Solar Radio Observatory / NAOJ, Nagano 384-1305, Japan*

## ABSTRACT

Analysis of the microwave data, obtained in the 17 GHz channel of the Nobeyama Radioheliograph during the M1.6 flare on 4th Nov 2010, revealed the presence of 11.8-min oscillations of the emitting plasma density. The oscillations decayed with the characteristic time of about 25-min. These oscillations are also well-seen in the variation of EUV emission intensity measured in the 335 Å channel of SDO/AIA. The observed properties of the oscillations are consistent with the properties of so-called SUMER oscillations, observed in the EUV and soft X-ray bands usually as a periodic Doppler shift. The accepted interpretation of SUMER oscillations is a standing slow magnetoacoustic wave. Our analysis presents the first direct observation of the slow magnetoacoustic oscillations in the microwave emission of a solar flare.

*Subject headings:* Sun: oscillations — Sun: corona — Sun: flares — Sun: radio radiation

## 1. Introduction

Quasi-periodic pulsations (QPP) in the emission generated in solar flares, with the periods ranging from a fraction of second to several minutes, have been intensively studied for several decades (see, e.g. Nakariakov & Melnikov 2009, for a recent review). One of the possibilities opened up by revealing the nature of QPP in flares is the diagnostics of physical conditions in flaring sites and mechanisms operating in them. Moreover, this diagnostics can be extended to stellar flares, which are also observed to have QPP in their radio, optical and soft X-ray light curves (e.g. Stepanov et al. 2001; Mathioudakis et al. 2003; Mitra-Kraev et al. 2005). The origin of the QPP is still not clear, while it is accepted that they can be produced by several mechanisms. Perhaps, one of the most understood possibility is the generation of QPP by magnetohydrodynamic (MHD) oscillations of coronal structures. Coronal MHD oscillations are well seen in various bands directly with the modern high time and spatial resolution instruments, which provide researchers with the ground for their identification in the flaring emission.

Standing longitudinal oscillations of coronal loops were first detected as the periodic Doppler shift of the emission lines Fe XIX and Fe XXI, with the formation temperature greater than 6 MK, with the SOHO/SUMER instrument (Wang et al. 2003; Wang et al. 2003). The mean observed oscillation period is  $17.6 \pm 5.4$  min. The oscillations are strongly damped, with the damping time about one period of the oscillation. In some cases, the intensity oscillations are seen. There is a quarter-period phase lag between the intensity and the Doppler shift oscillations. The oscillations are usually observed in association with the soft X-ray brightenings, sometimes up to the M-class flares (Wang et al. 2007). Similar Doppler-shift oscillations during solar flares in emission lines of SXV and Ca XIX, with the formation temperature 12–14 MK, with Yohkoh/BCS were reported by Mariska (2006, 2005). In cooler coronal emission lines, similar oscillations were detected with Hinode/EIS (Mariska et al. 2008).

The compressible nature of the longitudinal oscillations and their long periods led to their interpretation in terms of standing slow magnetoacoustic oscillations damped because of high thermal conduction (Ofman & Wang 2002). A series of numerical studies (e.g. Nakariakov et al. 2004; Mendoza-Briceño et al. 2004; Tsiklauri et al. 2004; Selwa et al. 2005; Taroyan et al. 2005; Ogrodowczyk & Murawski 2007; Selwa et al. 2007; Gruszecki & Nakariakov 2011), accounting for various additional physical effects including viscosity, 2D and 3D geometry, stratification, nonlinear steepening and mode coupling, demonstrated the robustness of this interpretation. In particular, the simulations showed that, depending upon whether the oscillations are triggered at one or both footpoints of a coronal loop, the fundamental mode and its second spatial harmonics can be effectively excited. The modes have different

structure of the oscillations at the loop apex: in the fundamental mode there is a node of the density perturbation and the maximum of the field-aligned velocity perturbation at the apex, while it is the other way around in the second harmonics. The phase speed of the longitudinal waves is the tube speed  $C_T = C_s C_A / \sqrt{C_s^2 + C_A^2}$ , where  $C_s$  and  $C_A$  are the sound and Alfvén speeds, respectively. The tube speed is subsonic and sub-Alfvénic. In a low-beta plasma the tube speed is just slightly lower than the sound speed, while in the case  $C_s = C_A$  the tube speed decreases to about  $0.7C_s$ . With the decrease in the Alfvén speed  $C_A < C_s$  the tube speed remains lower than the Alfvén speed.

Slow magnetoacoustic oscillations can be also observed in the non-thermal emission of solar and stellar flares. The possible mechanisms are the periodic triggering of magnetic reconnection by the modulation of the physical conditions in the vicinity of the reconnection site (Chen & Priest 2006), the modification of the spectral maximum of the gyrosynchrotron emission in the regime of the Razin suppression because of the periodic modulation of the electron plasma frequency (Nakariakov & Melnikov 2006), and the direct modulation of the emission intensity because of the change of the concentration of the emitting plasma. However, so far these theoretical possibilities have been without observational confirmation. In this Letter, we demonstrate, for the first time, the presence of longitudinal oscillations in the free-free microwave emission in a solar flare.

## 2. Observations

We have examined the flare loops produced by a M1.6 flare which occurs at south-east limb on 2010 Nov 4th. For this study, we used 17 GHz and 34 GHz data observed with Nobeyama Radioheliograph (NoRH; Nakajima et al. 1994; Takano et al. 1997) and 335 Å EUV data observed with Atmospheric Imaging Assembly (AIA; Lemen et al. 2011) onboard Solar Dynamics Observatory. Microwave data has a spatial resolution of 10 " and a time cadence of 10 seconds. AIA data has a spatial resolution of 1.2 " and a 12 seconds time cadence. AIA 335 Å channel contains a contribution from Fe XVI with the peak forming temperature of 2.5 MK for the flare (Lemen et al. 2011).

Figure 1 shows time profiles of the flare in soft X-rays taken with GOES satellite (top) and radio fluxes at 17 and 34 GHz (bottom). The flare starts at 23:55, peaks at 23:57 UT, and then gradually decays. The fluxes at 17 and 34 GHz vary with same pattern during flare process but the difference of scale between them clearly changes as follows: for the flare peak, 17 GHz flux is larger than 34 GHz and then decrease less than 34 GHz, and finally both fluxes become comparable with each others. It implies that only in the flare peak the radio emission is generated by gyrosynchrotron motion of accelerated electrons, while in the long

decay phase, thermal free-free dominate for the radio emission. Nobeyama Radiopolarimeter (NoRP; Nakajima et al. 1985), that observes the Sun in the 1, 2, 3.75, 9.4, 17, and 35 GHz channels, supports it with the same aspect at the high frequencies where the plasma becomes optically thin.

In Figure 2, we present spatial features of radio emission sources associated with the flare loops. Figure 2a exhibits the AIA 335 Å image taken at 00:30 UT and the brightness temperature ( $T_B$ ) contours of NoRH 17 and 34 GHz. Figure 2b shows NoRH 17 GHz  $T_B$  map with a contour of EUV flare loops observed by AIA 335 Å channel. The flare loops are coincided with the microwave source. The top of the flare loops emanate strong EUV emission continuously through the whole flare procedure. In Figure 3, we plotted the variation of the maximum counts recorded in the AIA 335 Å channel for the flare region. Since the top of the flare loops is the dominant source during the flare, this plot reflects the intensity variation of the flare loop-top. Interestingly, it shows an obvious decaying oscillation pattern after the flare peak time. Unfortunately, we couldn't confirm it in AIA 131 and 94 Å channel, where the peak of the temperature response is higher than 7 MK, due to the saturation effect on the top of the flare loops.

The NoRH observation at two frequencies allows us to derive a spectral index  $\alpha$  for a spatially resolved region such as the loop top or loop footpoint. The index  $\alpha$  is given by the ratio of the fluxes obtained at 17 and 34 GHz,  $\alpha = \log(F_{17GHz}/F_{34GHz})/\log(17/34)$ . For the top of the arcade (the white box in Figure 2b), the derived index  $\alpha$  is close to 0 within range of  $-0.2 \sim 0.7$  during the decay phase. It imply that the radio emission in this region comes from an optically thin plasma (Dulk 1985).

We estimated the plasma temperature of the flare loops using the ratio of the GOES two channels (1–8 Å and 0.5–4 Å ). Although GOES satellite observes the full Sun, it is reasonable to use it in our analysis because only this flaring loop is the predominant source for the increasing X-ray flux during the flare time. Using GOES widget, we derived the temperature in the flare loops (White et al. 2005). The temperature response function of each filter is derived using the coronal abundances in CHIANTI 6.0.1 (Dere et al. 1997, 2009). The estimated peak temperature is 18 MK. Then, the temperature gradually decreases to about 7 MK (top panel of Figure 3). Since we are focusing on the top of the flare loops that appears in microwave imaging data, we do not use GOES emission measure estimated over the whole flare.

### 3. Electron Density

To derive the electron number density of the flare loop-top region, we used the brightness temperature obtained at 17 GHz of NoRH and the estimated plasma temperature by the GOES two channels. Based on the observations, we assume that in the top of the flare loops the free-free emission from the optically thin thermal plasma (the optical depth  $\tau_\nu \ll 1$ ) is dominant. According to the radiative transfer at the radio frequency (e.g. Dulk 1985), the relation between the brightness temperature  $T_B$  and the plasma temperature  $T$  is given as

$$T_B = T\tau_\nu, \quad (1)$$

where  $\tau_\nu$  is

$$\tau_\nu = \frac{9.786 \times 10^{-3}}{\nu^2} \ln\Lambda \frac{EM}{T^{3/2}}. \quad (2)$$

$EM$  is the emission measure ( $EM = \int_z N^2 dz$ ) and  $\log \Lambda$  is the Coulomb logarithm ( $\log \Lambda = \log[4.7 \times 10^{10}(T/\nu)]$ ). The path on the line-of-sight ( $z$ ) is assumed as the half of the distance between footpoints of the flare loops seen in the contour on Figure 2b ( $z = 25$  Mm). Substituting these observational results to equation (2), we derived  $EM$  and then estimated the number density of electrons at the top of the flare loops. The middle panel of Figure 4 shows the resulted electron density variation with time during the whole flare process. Since the peak emission of the flare is not caused by the thermal free-free but by the strong gyrosynchrotron emission, the density estimation related with the flare peak time cannot be analyzed as a physical parameter in our assumptions. Therefore we have examined the density estimated from 00:00 UT (the vertical dashed line in Figure 4) to 00:50 UT, from the time when the emission only come from the free-free transition to just before the next flare start. From 00:00 UT, the density fluctuations come into sight and its amplitude gradually diminish with time.

### 4. Decaying oscillations

The time dependence of the electron density derived by the radio emission (middle panel of Figure 4), as well as the EUV emission (Figure 3), shows a decaying long-period oscillatory pattern. To emphasise the oscillatory pattern we de-trend the observational curve by subtracting the same curve averaged by 500 s. Best-fitting the de-trended observational curve from 00:00 UT by a decaying harmonic function gives us the parameters of this oscillation: the period of 710 s and the decay time of 1500 s. The amplitude of the oscillation is about 6% of the background in the beginning of the oscillations. The result of this approximation, shown in the bottom panel of Figure 4, demonstrates a rather good agreement between the

observational and the best-fitted curve. Also, we see that the amplitude of short-period fluctuations from this decaying harmonic curve decreases with time. We would like to stress that the detection of the oscillation is not sensitive to the specific choice of the time scale in the boxcar de-trending, as the oscillatory pattern is clearly visible in the original signal.

## 5. Discussion

We have demonstrated that there is an electron density QPP oscillation with 11.8-min period and 25-min decay time, and the amplitude of several percent of the background in the flare loops. This electron density have been deduced by radio emission observed by 17 GHz Nobeyama Radioheliograph and it is first evidence of radio observation for the long-period oscillation of the thermal emission produced by a flare. The QPP is also well-pronounced in the EUV 335 Å signal obtained with SDO/AIA. The observed parameters of the oscillation, the period and decay time, as well as its compressive nature, are similar to the compressive oscillations of coronal loops, known as SUMER oscillations.

Following the interpretation of SUMER oscillations as a standing slow magnetoacoustic wave (Ofman & Wang 2002) we estimate parameters of the observed oscillation. Consider two lowest spatial harmonics. In the slow wave the density is perturbed because of the spatial redistribution of the matter mainly along the magnetic field. In a loop it corresponds to the field-aligned movement of the plasma from one footpoint to the other (in the fundamental mode) or from both the footpoint to the apex (in the second standing harmonics). Taking the loop height of about 50'' and assuming that the loop is of semi-circular shape, we get its length of about 115 Mm. The fundamental mode has the wavelengths of  $\lambda_1 \approx 2 \times 115$  Mm. The wavelength of the second spatial harmonics is  $\lambda_2 \approx 115$  Mm. Estimating the phase speeds as the ratio of the wavelengths to the value of the period, 710 s, we obtain about 320 km/s for the fundamental mode and 160 km/s for the second spatial harmonics. The plasma temperature associated with the 335 Å channel is about 2.5 MK, which gives us the sound speed of about  $C_s \approx 240$  km/s. This value is consistent with the phase speed required for the interpretation of the oscillations in terms of the fundamental acoustic mode (see, e.g. Wang et al. 2007).

On the other hand, temperature diagnostics performed with the use of GOES data shows that the plasma has higher temperature, about 7 MK (see Sec. 3). For this temperature, the sound speed  $C_s$  is greater than 380 km/s. In this case, the decrease in the phase speed can be attributed to the relatively low value of the Alfvén speed  $C_A$ , of the value of the sound speed. This reduces the phase speed of the longitudinal waves  $C_T$  to the required value if  $C_A \approx C_s$ . This result is consistent with the estimations of the plasma beta (Shibasaki 2001,

2008), which show that in flaring loops this parameter could reach or even exceed unity, giving us the tube speed of the required value. The fact that the oscillations are well seen in the 335Å channel can be attributed to the effect of the crosstalk from the 131 Å channel (Lemen et al. 2011). The oscillation is not seen in hotter channels of AIA because of the saturation.

Also, if the oscillation of the emission detected in the 335Å channel is produced by the cooler plasma, this oscillation can be induced by the slow magnetoacoustic oscillations in the hotter loops. One possible scenario is based upon the possibility that hot and cool loops form loop bundles, with the steep temperature gradient in the transverse direction (e.g. King et al. 2003). Slow magnetoacoustic oscillations cause not only longitudinal, but also transverse motions of the plasma (Gruszecki & Nakariakov 2011). These transverse motions grow with the increase in beta, and are significant when beta is about unity. Hence, standing slow magnetoacoustic oscillations channeled by hotter loops would naturally affect the cooler plasma in the cooler loops situated nearby, and hence may be visible in the cooler temperature emission.

Thus, we conclude that our results give the first direct observational evidence of slow magnetoacoustic waves in the solar corona in the thermal radio emission, similar to the phenomenon known as SUMER oscillations.

The observed gradual decrease in the electron density fluctuations from the decaying harmonic pattern can be attributed to the decay of the compressible turbulence in the flaring site, excited by the flare, and should be subject to further investigation.

The work was supported by t...

## REFERENCES

- Boerner et al. 2011, Sol. Phys.
- Chen, P. F., & Priest, E. R. 2006, Sol. Phys., 238, 313
- Dere, K. P., Landi, E., Mason, H. E., Monsignori Fossi, B. C., & Young, P. R. 1997, A&ASeries, 125, 149
- Dere, K. P., Landi, E., Young, P. R., Del Zanna, G., Landini, M., & Mason, H. E. 2009, A&A, 498, 915
- George A. Dulk 1985, Ann.Rev.Astron.Astrophys., 23, 169

- Freeland, S. L. & Handy, B. N. 1998, *Sol. Phys.*, 182, 497
- Gruszecki, M., & Nakariakov, V. M. 2011, *A&A*, 536, A68
- Kano, R. et al. 2004, *ASP Conf. Ser.*, 325, 15
- King, D. B., Nakariakov, V. M., Deluca, E. E., Golub, L., & McClements, K. G. 2003, *A&A*, 404, L1
- Lemen et al. 2011, *Sol. Phys.*
- Mariska, J. T. 2006, *ApJ*, 639, 484
- Mariska, J. T. 2005, *ApJ*, 620, L67
- Mariska, J. T., Warren, H. P., Williams, D. R., & Watanabe, T. 2008, *ApJ*, 681, L41
- Mathioudakis, M., Seiradakis, J. H., Williams, D. R., Avgoloupis, S., Bloomfield, D. S., & McAteer, R. T. J. 2003, *A&A*, 403, 1101
- Mendoza-Briceño, C. A., Erdélyi, R., & Sigalotti, L. D. G. 2004, *ApJ*, 605, 493
- Mitra-Kraev, U., Harra, L. K., Williams, D. R., & Kraev, E. 2005, *A&A*, 436, 1041
- Nakariakov, V. M., & Melnikov, V. F. 2009, *Space Sci. Rev.*, 149, 119
- Nakariakov, V. M., & Melnikov, V. F. 2006, *A&A*, 446, 1151
- Nakariakov, V. M., Tsiklauri, D., Kelly, A., Arber, T. D., & Aschwanden, M. J. 2004, *A&A*, 414, L25
- Nakajima, H., Sekiguchi, H., Sawa, M., Kai, K., & Kawashima, S. 1985 *PASJ*, 37, 163
- Nakajima, H., et al. 1994, *Proc. of the IEEE*, 82, 701
- Ofman, L., & Wang, T. 2002, *ApJ*, 580, L85
- Ogrodowczyk, R., & Murawski, K. 2007, *A&A*, 467, 311
- Selwa, M., Murawski, K., & Solanki, S. K. 2005, *A&A*, 436, 701
- Selwa, M., Ofman, L., & Murawski, K. 2007, *ApJ*, 668, L83
- Shibasaki, K. 2001, *ApJ*, 557, 326
- Shibasaki, K. 2008, *Plasma and Fusion Research*, 2, 1012



- Stepanov, A. V., Kliem, B., Zaitsev, V. V., Fürst, E., Jessner, A., Krüger, A., Hildebrandt, J., & Schmitt, J. H. M. M. 2001, *A&A*, 374, 1072
- Takano, T. et al. 1997, in *Coronal Physics from Radio and Space Observations: Proceedings of the CESRA Workshop* (Springer, Berlin)
- Taroyan, Y., Erdélyi, R., Doyle, J. G., & Bradshaw, S. J. 2005, *A&A*, 438, 713
- Tsiklauri, D., Nakariakov, V. M., Arber, T. D., & Aschwanden, M. J. 2004, *A&A*, 422, 351
- Wang, T., Innes, D. E., & Qiu, J. 2007, *ApJ*, 656, 598
- Wang, T. J., Solanki, S. K., Curdt, W., Innes, D. E., Dammasch, I. E., & Kliem, B. 2003, *A&A*, 406, 1105
- Wang, T. J., Solanki, S. K., Innes, D. E., Curdt, W., & Marsch, E. 2003, *A&A*, 402, L17
- White, S.M., Thomas, R. J. & Schwartz, R. A. 2005, *Sol. Phys.*, 227, 231

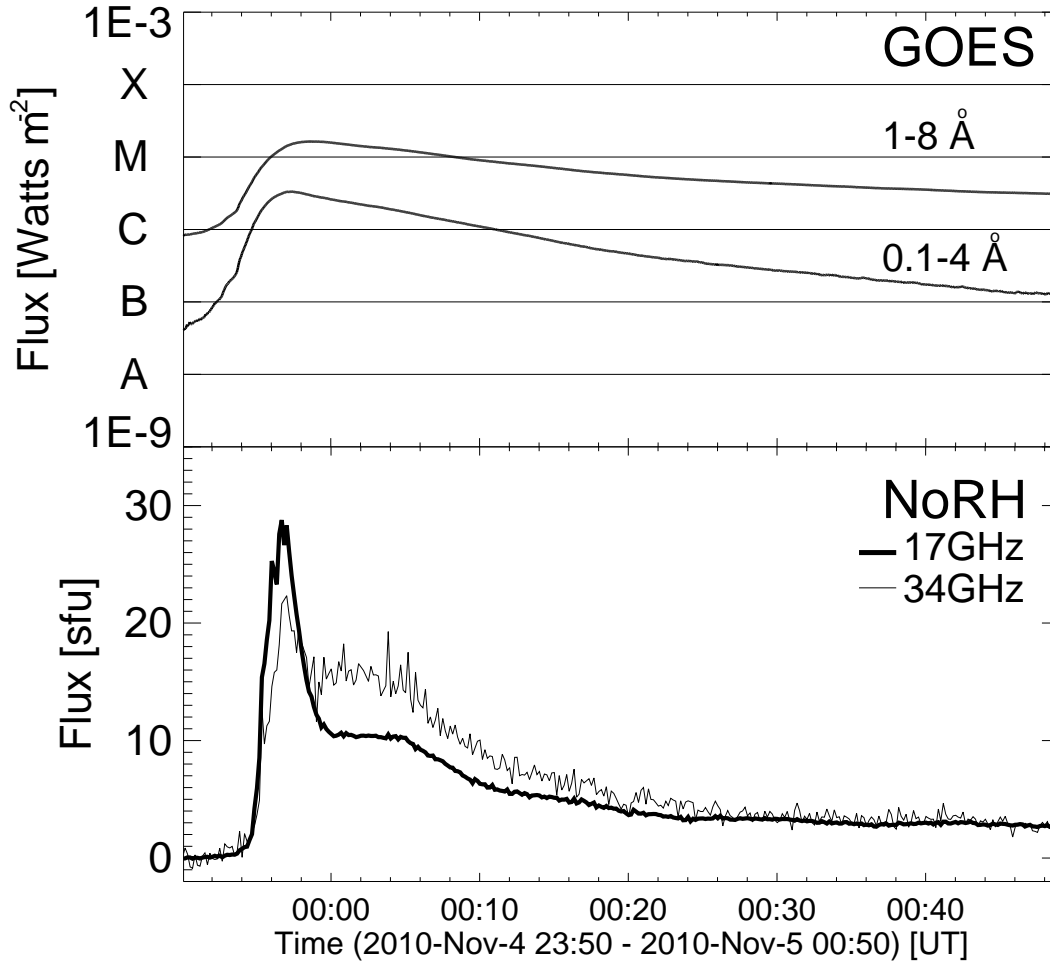


Fig. 1.— Time profile of GOES X-ray (top) and NoRH 17 and 34 GHz (bottom) flux during a M1.6 flare occurred in 2010 Nov 4th. NoRH flux at each frequency is estimated over the field of view of Figure 2.

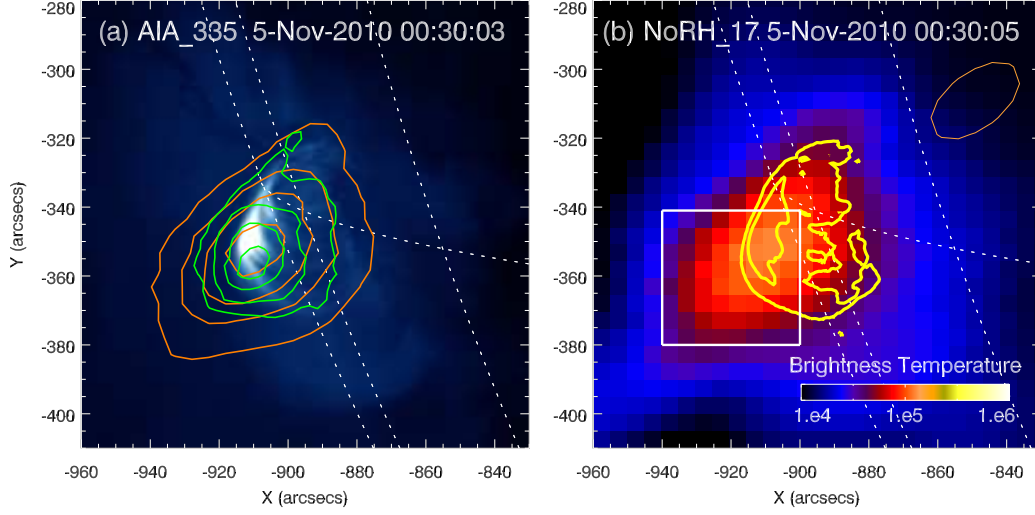


Fig. 2.— Images for the flare loops at around 00:19 UT. (a) AIA 335 Å channel image with contours of  $T_B$  at NoRH 17 GHz (orange) and 34 GHz (green). The levels of contours are 35, 55, 75, and 95 % of peak  $T_B$  for each frequency. (b) NoRH 17 GHz  $T_B$  map with contour of flare loop arcade observed by AIA 335 Å channel. A beam size at 17 GHz appears in a yellow circle and a white box indicates the region where the electron density is estimated. (A color version of this figure is available in the online journal.)

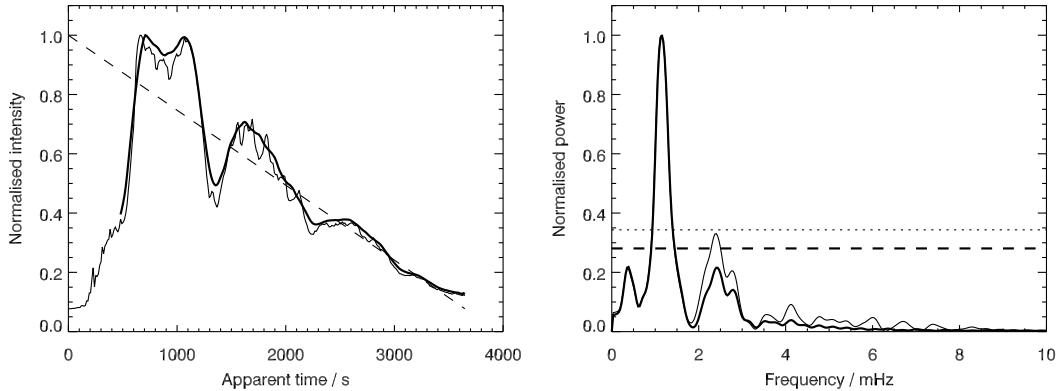


Fig. 3.— Time profile of maximum counts obtained by AIA 335 Å channel in the flare loops

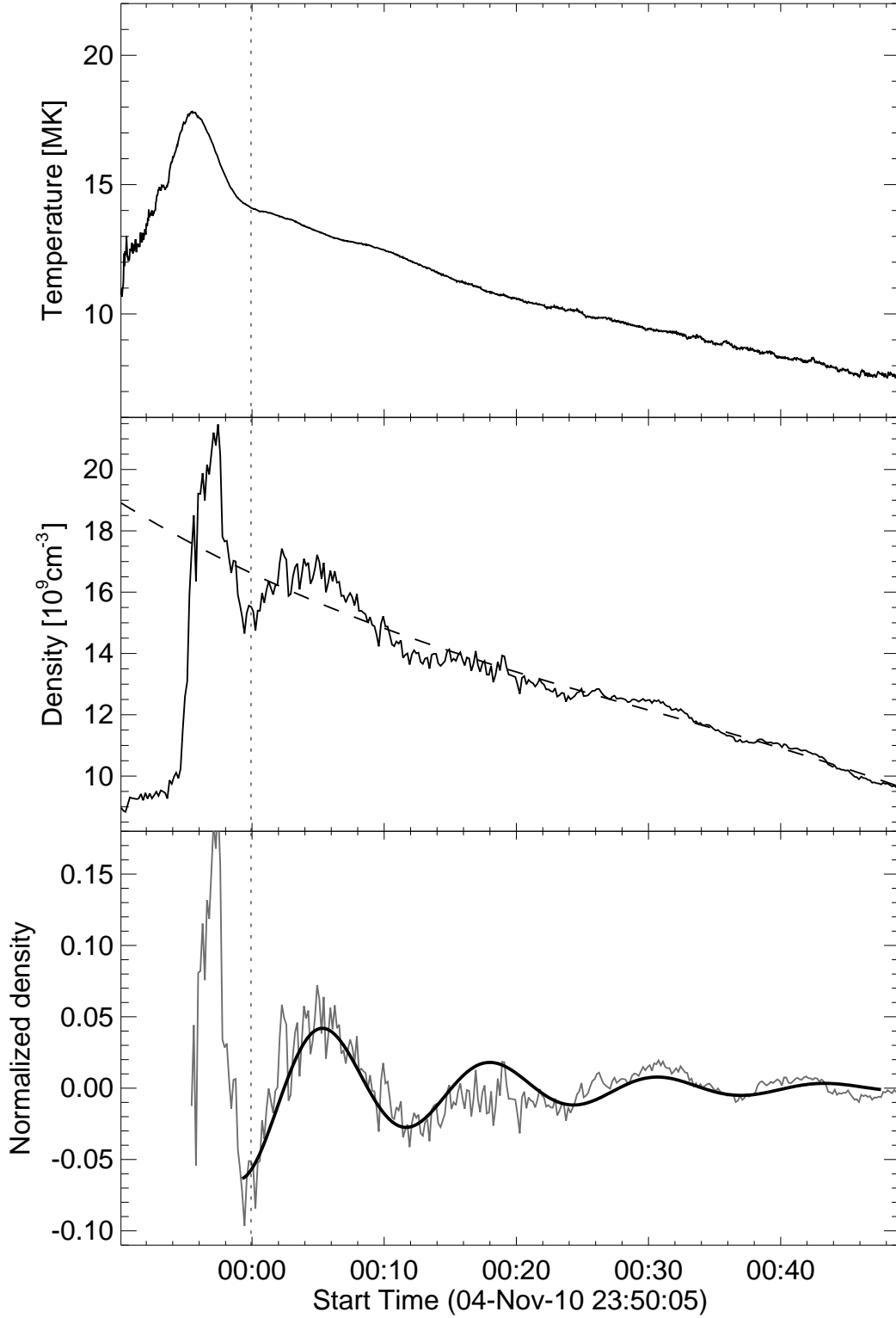


Fig. 4.— Time profile of temperature estimated by GOES two channels (top), electron number density derived by this temperature and  $T_B$  at 17 GHz (mid), and a best fit on the normalized electron number density (bottom). Free-free emission become predominant than gyrosynchrotron emission from 00:00 UT (vertical dashed-line).